

# A VLT/FLAMES survey for massive binaries in Westerlund 1: I. first observations of luminous evolved stars<sup>\*</sup>

B. W. Ritchie<sup>1,2</sup>, J. S. Clark<sup>1</sup>, I. Negueruela<sup>3</sup>, and P. A. Crowther<sup>4</sup>

<sup>1</sup> Department of Physics and Astronomy, The Open University, Walton Hall, Milton Keynes MK7 6AA, United Kingdom

<sup>2</sup> IBM United Kingdom Laboratories, Hursley Park, Winchester, Hampshire SO21 2JN, United Kingdom

<sup>3</sup> Departamento de Física, Ingeniería de Sistemas y Teoría de la Señal, Universidad de Alicante, Apdo. 99, 03080 Alicante, Spain

<sup>4</sup> Department of Physics and Astronomy, University of Sheffield, Sheffield S3 7RH, United Kingdom

Accepted ??? Received ???

## ABSTRACT

**Aims.** Multiwavelength observations of the young massive cluster Westerlund 1 have revealed evidence for a large number of OB supergiant and Wolf-Rayet binaries. However, in most cases these findings are based on the detection of secondary binary characteristics, such as hard X-ray emission and/or non-thermal radio spectra and hence provide little information on binary properties such as mass ratio and orbital period. To overcome this shortcoming we have initiated a long temporal baseline, multi-epoch radial velocity survey that will provide the first direct constraints on these parameters.

**Methods.** VLT/FLAMES+GIRAFFE observations of Wd1 were made on seven epochs from late-June to early-September 2008, covering  $\sim 35$  confirmed members of Wd1 and  $\sim 70$  photometrically-selected candidate members. Each target was observed on a minimum of three epochs, with brighter cluster members observed on five (or, in a few cases, seven) occasions. Individual spectra cover the 8484-9001Å range, and strong Paschen-series absorption lines are used to measure radial velocity changes in order to identify candidate binary systems for follow-up study.

**Results.** This study presents first-epoch results from twenty of the most luminous supergiant stars in Wd1. Four new OB supergiant members of Wd1 are identified, while statistically significant radial velocity changes are detected in  $\sim 60\%$  of the targets. W43a is identified as a short-period binary, while W234 and the newly-identified cluster member W3003 are probable binaries and W2a is a strong binary candidate. The cool hypergiants W243 and W265 display photospheric pulsations, while a number of early-mid B supergiants display significant radial velocity changes of  $\sim 15\text{--}25\text{km s}^{-1}$  that we cannot distinguish between orbital or photospheric motion in our initial short-baseline survey. When combined with existing observations, we find 30% of our sample to be binary (6/20) while additional candidate binaries support a binary fraction amongst Wd1 supergiants in excess of  $\sim 40\%$ , a figure that is likely to increase as further data become available.

**Key words.** stars: evolution - supergiants - stars: binaries: general - techniques: radial velocities

## 1. Introduction

Despite direct observational confirmation of stars with dynamical masses in excess of  $80 M_{\odot}$  (e.g. Rauw et al. 2005; Schnurr et al. 2008), the production of massive stars is poorly understood, largely as a result of their intrinsic rarity, apparent rapidity of formation and extreme extinction due to veiling by their natal envelopes. Moreover, their production is problematic on theoretical grounds, primarily because accretion rates must be both extreme in order to build the star and yet must overcome the resultant radiation pressure. Hence it is not clear if the process is simply a scaled up version of low mass formation or whether it proceeds by a different mechanism (e.g. Bonnell & Bate 2005 and refs. therein). An additional problem is that even if

radiation pressure can be overwhelmed, sufficient material must be present to accrete from in order to yield the stars themselves (Davies et al. 2006).

Nevertheless, several differing scenarios have been advanced to surmount these difficulties. Disc mediated accretion has been suggested to overcome radiation pressure (Yorke & Sonnhalter 2002) but sufficient material must still be supplied to the protostar. One mechanism proposed to accomplish this is competitive accretion onto high mass protostars in cluster cores (Bonnell & Bate 2006). An alternative, which also circumvents the constraints imposed by radiation pressure, is that massive stars form as the result of stellar mergers (e.g. Bonnell et al. 1998, Davies et al. 2006), though both processes may be relevant (Bonnell & Bate 2005).

While direct observations of *in situ* massive star formation are technically highly challenging, significant observational constraints on this process exist. For instance, the finding that massive stars appear to form in clusters (e.g. Zinnecker et al. 1993, Clarke et al. 2000) appears difficult

Send offprint requests to: B.W. Ritchie, e-mail: b.ritchie@open.ac.uk

<sup>\*</sup> This work is based on observations collected at the European Southern Observatory, Paranal Observatory under programme ID ESO 81.D-0324A...E.

to reconcile with turbulent fragmentation of the molecular cloud leading to the production of protostellar cores, since the resultant clump masses are significantly lower than required to form massive O stars (Clark & Bonnell 2004). A second constraint is provided by the observed binary fraction and properties of massive stars; competitive accretion predicts their formation via accretion onto wide low mass systems leading to massive close binaries ( $\sim 1$  AU; Bonnell & Bate 2005), while massive star formation via stellar mergers leads to a reduction in the number of primordial binaries, and hence requires a very high initial fraction. As such, recent observational results demonstrating a large binary fraction amongst massive stars have the potential to directly test current theories of star formation (e.g. García & Mermilliod 2001, Kiminki et al. 2007, Sana et al. 2008, Bosch et al. 2009, Clark et al. 2009a). The properties of these populations, such as the distribution of eccentricities, mass ratio and orbital separations place stringent constraints on the production rates and channels of both high and low mass X-ray binaries - and ultimately double degenerate systems - as well as both Type Ib/c and blue Type II supernovae and potentially Gamma Ray Bursters (Kobulnicky & Fryer 2007 and refs. therein).

The starburst cluster Westerlund 1 (hereafter Wd1; Westerlund 1961) contains a rich population of massive, evolved stars including Wolf-Rayets, OB supergiants, yellow hypergiants, a luminous blue variable, and red supergiants (Clark et al. 2005). This unique population has been the subject of extensive study in recent years at radio (Dougherty & Clark 2008), infrared (Crowther et al. 2006), visual (Clark & Negueruela 2002; Clark et al. 2005; Negueruela et al. 2009) and X-ray wavelengths (Skinner et al. 2006; Clark et al. 2008). These studies have shown that 17 of the 24 identified Wolf-Rayet stars are binary (Crowther et al. 2006; Clark et al. 2008), while photometric (Bonanos 2007) and X-ray (Clark et al. 2008) studies also imply a significant binary fraction amongst the transitional OB supergiants that are the evolutionary precursors of the Wolf-Rayet population. However, the existing studies are largely based on secondary binary diagnostics such as the presence of non-thermal radio emission, hard and/or high luminosity X-ray emission and a significant near-mid IR excess, all of which are thought to be observational signatures of Colliding Wind Binaries (CWBs). Moreover, the single epoch observations used to identify CWBs provide little information on the nature of the binary, save that the secondary is expected to be massive enough to support a powerful stellar wind<sup>1</sup>. Binaries have been directly detected in only a few cases, e.g. the eclipsing binaries W13 and W36 (Bonanos 2007) or the double-lined spectroscopic binary W10 (Negueruela et al. 2009).

Consequently we have initiated a long temporal baseline, multi-epoch VLT/FLAMES spectroscopic radial velocity (RV) survey designed to identify and characterise binaries within Wd1. The sensitivity offered is high enough to identify both short- and long-period binaries and is sensitive to low mass companions within short period systems. This is the first of three planned papers, describing target selection, data reduction and analysis for our

**Table 1.** Summary of observations of the four sets of targets.

Date	MJD <sup>a</sup>	$\Delta t^b$	Targets	Integration time
20/06/2008	54637.190	—	Faint 1	3×895s
	54637.230	—	Faint 2	3×895s
29/06/2008	54646.185	—	Bright	2×600s
	54646.224	—	Faint 3	3×895s
18/07/2008	54665.036	18.85	Bright	2×600s
	54665.065	18.84	Faint 3	3×895s
	54665.104	27.87	Faint 2	3×895s
	54665.144	27.95	Faint 1	3×895s
24/07/2008	54671.134	6.10	Bright	2×600s
14/08/2008	54692.042	20.91	Bright	2×600s
	54692.073	27.01	Faint 3	3×895s
17/08/2008	54695.094	29.99	Faint 2	3×895s
	54695.133	29.99	Faint 1	3×895s
04/09/2008	54713.011	20.97	Bright	2×500s

<sup>a</sup>The modified Julian day (MJD) is given at the midpoint of the sequence of integrations.

<sup>b</sup>The time since the target field was last observed.

survey, and presenting the first results from a subset of the VLT/FLAMES dataset containing a sample of luminous, evolved supergiants observed on five epochs between 29/06/2008 and 04/09/2008. Paper II will present analysis of our full dataset<sup>2</sup>, consisting of  $\sim 105$  spectroscopically- and photometrically-selected targets observed on a minimum of six epochs during 2008 and 2009. A final paper will present follow-up observations and numerical modeling of the observed RV variability (*cf.* Kobulnicky & Fryer 2007) aimed at placing limits on the close, high-mass binary fraction, the orbital and mass-ratio distributions and the permitted formation channels for low- and high-mass X-ray binaries within Wd1.

## 2. Observations & data reduction

Observations were made using the Fibre Large Array Multi Element Spectrograph (FLAMES; Pasquini et al. 2002), located on VLT UT2 *Kueyen* at Cerro Paranal. FLAMES provides multi-object spectroscopy using the GIRAFFE medium-high resolution and/or UVES high resolution spectrographs, with the red arm of UVES fed by up to eight fibres and the MEDUSA mode of GIRAFFE allowing simultaneous observation of up to 132 separate objects<sup>3</sup>. Our observations use GIRAFFE in MEDUSA mode, but the high degree of crowding towards the core of Wd1 means that we cannot simultaneously allocate fibres to all spectroscopically-confirmed cluster members due to limitations imposed by the physical size of the MEDUSA fibres and the need to avoid collisions. Instead we use *FPOSS* (the FLAMES Fibre Positioner Observation Support Software) to optimally allocate fibres to targets drawn from four lists of candidates:

<sup>1</sup> Wind-photosphere interaction may also result in X-ray emission in systems where the secondary lacks a strong wind (e.g. the O9V + B1–1.5V binary CPD -41°7742; Sana et al. 2005).

<sup>2</sup> Additional data during 2009 is anticipated under ESO program ID 383.D-0633.

<sup>3</sup> Two GIRAFFE Integral Field Unit modes are also available.

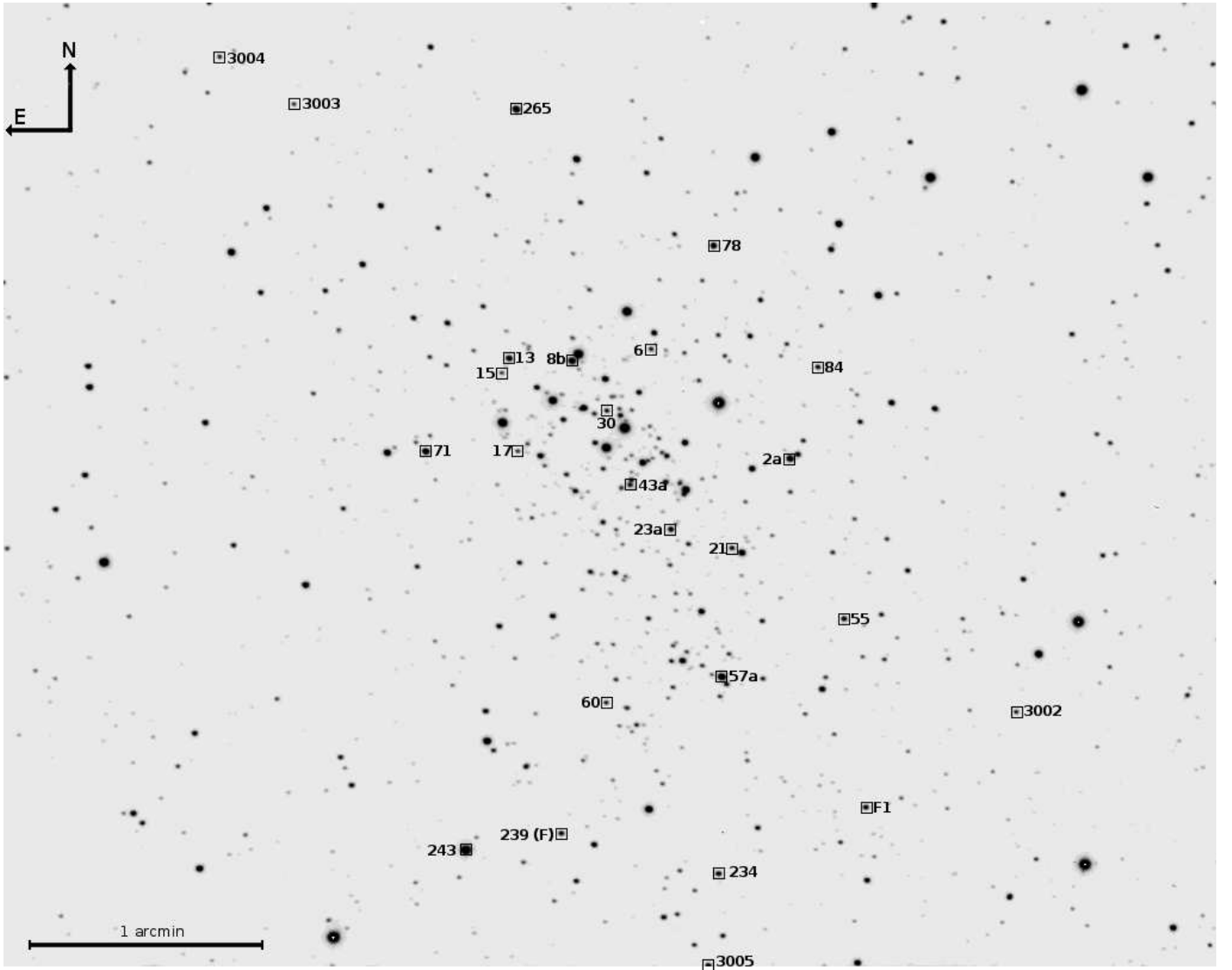


**Fig. 1.** VLT/FORS1 R-band finding chart ( $\sim 0.6''$  seeing) for the targets listed in Table 2. The field of view is  $\sim 4'$  square, corresponding to  $\sim 6$ pc at an assumed cluster distance of  $\sim 5$ kpc (Clark et al. 2005).

- Known cluster members catalogued by Westerlund (1987). The brightest OB and transitional supergiant members of Wd1 are assigned the highest priority for fibre allocation, while other catalogued OB I/II stars are assigned moderate priority. Yellow hypergiants and the Wolf-Rayet population are assigned low priority; the YHGs are presumed too large to allow a close companion, while the binary fraction of the Wolf-Rayet population has been examined by Crowther et al. (2006).
- Candidate cluster members with SuSI2 photometry (Clark et al. 2005). These targets are located in a  $5.5 \times 5.5$ -arcminute field centred just north-east of the core of Wd1. These are again assigned moderate priority, with increasing likelihood of selection away from the highest-priority OB supergiants in the cluster core.
- Bright stars away from the cluster core with WFI photometry (Baade et al. 1999) suggestive of cluster membership. These are assigned low priority, but still have a high probability of selection during fibre configura-

tion due to the lack of alternative targets away from the cluster core.

- Objects around the cluster core that are likely to be members based on their general colour, but have no existing photometry or spectroscopy. These targets are assigned a low priority for fibre configuration and serve as backup targets for fibres that cannot be allocated in any other way.

Four lists of targets were generated using *FPOSS*. A *bright* list, observed on five epochs in 2008, contains 17 of the brightest confirmed cluster members and five candidate members located towards the core of Wd1 for which no photometry or spectroscopy exists. In addition, three *faint* lists, observed on three epochs, contain a further 17 known cluster members, 58 photometrically-selected candidates (28 with SuSI2 photometry and 30 with WFI photometry) and 16 candidates for which no existing observations are available. A summary of all the observations is given in Table 1. Each target list also includes  $\sim 10$  fibres that were used to obtain sky spectra. Despite being assigned low priority,

**Table 2.** List of targets.

ID	Spectral Type	RA (J2000)	Dec (J2000)	$R^a$	$I^a$	Field <sup>b</sup>	Notes <sup>c</sup>
W2a	B2Ia <sup>e</sup>	16 46 59.71	-45 50 51.1	14.23	11.73	Br.	A
W8b	B1.5Ia <sup>e</sup>	16 47 04.95	-45 50 26.7	–	–	Br.	
W13	B0.5Ia <sup>+</sup> +OB <sup>e</sup>	16 47 06.45	-45 50 26.0	14.63	12.06	Br.	X, E (9.20 day)
W21	B0.5Ia <sup>e</sup>	16 47 01.10	-45 51 13.6	15.56	12.74	Br.	A
W23a	B1.5Ia <sup>e</sup>	16 47 02.57	-45 51 08.7	14.91	12.07	Br.	A
W30a	O9–B0.5Ia bin <sup>f</sup>	16 47 04.11	-45 50 39.0	15.80	13.20	Br.	X
W43a	B0Ia <sup>e</sup>	16 47 03.54	-45 50 57.3	15.22	12.26	Br.	A
W55	B0Iab <sup>g</sup>	16 46 58.40	-45 51 31.2	15.25	12.67	Br./1	A
W60	B0Iab <sup>e</sup>	16 47 04.13	-45 51 52.1	15.96	13.28	Br.	A
W71	B2.5Ia <sup>e</sup>	16 47 08.44	-45 50 49.3	14.06	11.16	Br./1	A
W78	B1Ia <sup>e</sup>	16 47 01.54	-45 49 57.8	14.54	12.04	Br.	A
W84	O9.5Ib <sup>e</sup>	16 46 59.03	-45 50 28.2	15.60	13.63	Br.	X?
W234	O9.5Ib	16 47 01.44	-45 52 35.0	–	–	Br./1	
W239 (F)	WC9d <sup>g</sup>	16 47 05.21	-45 52 25.0	15.39	12.90	Br.	X, A
W243	LBV (A3Ia <sup>+</sup> ) <sup>h</sup>	16 47 07.55	-45 52 28.5	–	–	Br.	A
W265	F5Ia <sup>+</sup> <sup>g</sup>	16 47 06.26	-45 49 23.7	13.62	10.54	Br.	A
W373	B0Iab	16 46 57.71	-45 53 20.0	<i>14.74</i>	<i>12.32</i>	Br.	A
W3002	B0Iab	16 46 54.24	-45 51 54.7	–	–	Br.	
W3003	B0Ib	16 47 11.60	-45 49 22.4	<i>16.21</i>	<i>13.31</i>	Br.	A
W3004	B0Iab	16 47 13.39	-45 49 10.5	<i>15.96</i>	<i>12.99</i>	Br.	A
W3005	O9.5Ib	16 47 01.69	-45 52 57.8	<i>15.39</i>	<i>12.97</i>	Br.	A
F1 <sup>d</sup>	M2II-III	16 46 57.84	-45 52 18.5	–	–	Br.	Field
W6a	O9–B0.5Ia bin <sup>f</sup>	16 47 03.04	-45 50 23.6	15.80	13.16	1	X, P (2.20 day)
W15	O9Ib <sup>e</sup>	16 47 06.63	-45 50 29.7	16.38	13.75	2	X, A
W17	O9Iab <sup>e</sup>	16 47 06.25	-45 50 49.2	16.19	13.56	1	X
W57a	B4Ia <sup>e</sup>	16 47 01.35	-45 51 45.6	13.83	11.13	1	A

<sup>a</sup>Photometric  $R$  and  $I$ -band photometric magnitudes are taken from Clark et al. (2005) or Bonanos (2007) where available. Values from Bonanos (2007) are listed in italics.

<sup>b</sup>Targets are listed as *Br.* for members of the *bright* list, or 1...3 for the *faint* target lists. The stars W6a, W15, W17 and W57a are not included in our main target list, but are discussed in the text.

<sup>c</sup>Stars are noted as **E**clipsing, **P**eriodic or **A**periodic variables (Bonanos 2007) and/or **X**-ray sources (Clark et al. 2008).

<sup>d</sup>The target F1 is a foreground star, and not a member of Wd1.

References: <sup>e</sup>Negueruela et al. (2008, 2009); <sup>f</sup>Clark et al. (2008); <sup>g</sup>Clark et al. (2005); <sup>h</sup>Ritchie et al. (2009).

two Wolf-Rayets, W239(F/WR77n) and W39b(G/WR77j), were included by the fibre allocation process, with W239 included in the *bright* targets list, while three targets are duplicated on the *bright* and *faint1* lists and are therefore observed seven times in total. With the exception of two of these duplicated objects (W71, B2.5Ia and W55, B0Iab), the transitional supergiant W57a (B4Ia, *faint1*), and the Wolf-Rayet W39b/G (WN7o, *faint2*), the known cluster members in the *faint* lists all have spectral classifications in the range O9II–B0Ib (Negueruela et al. 2009), while visual inspection of the photometrically-selected targets suggest they are predominantly reddened late-OI/II stars that are likely *bona fide* members of Wd1 along with a number of field stars with colours similar to the reddened supergiants: full spectral classification will be given in Paper II. As many of our photometrically-selected targets are uncatalogued by Westerlund (1987), we name targets that are subsequently confirmed as members of Wd1 as W2xxx if they are selected using photometry from Clark et al. (2005) and W3xxx otherwise, where in both cases the final three digits count upwards from 001.

Due to the high degree of reddening towards Wd1 ( $A_v \sim 12$ ; Clark et al. 2005) the expected signal-to-noise ratio at the blue end of the spectrum would be too poor to allow high-precision RV measurements to be obtained. Instead,

we use the near-IR atmospheric window at  $\sim 8350 - 9000\text{\AA}$ , which covers a number of strong, well defined Paschen-series absorption lines in the spectra of OB supergiants (Clark et al. 2005; Negueruela et al. 2009). This region is free from telluric features, and the line formation region deep in the stellar photosphere implies the observed absorption lines should be free from wind contamination<sup>4</sup>. The GIRAFFE spectrograph was therefore used with setup HR21 covering the 8484–9001 $\text{\AA}$  range with  $R = \lambda/\Delta\lambda \sim 16200$ . Two 600s integrations were used for the bright targets, while three 895s integrations were used for the faint targets. The FLAMES data were bias-subtracted, flat-fielded to correct for pixel-to-pixel variation and fibre transmission differences, and wavelength-calibrated using version 2.5.3 of the FLAMES-GIRAFFE pipeline<sup>5</sup> with version 4.1.0 of the Common Pipeline Library (CPL), with individual spectra extracted from the final pipeline frames

<sup>4</sup> To test this hypothesis we have calculated non-LTE model atmosphere synthetic spectra for a range of parameters, with the synthetic spectra showing no evidence for wind contamination, even with mass loss rates an order of magnitude above expected values.

<sup>5</sup> <http://www.eso.org/sci/data-processing/software/pipelines/>

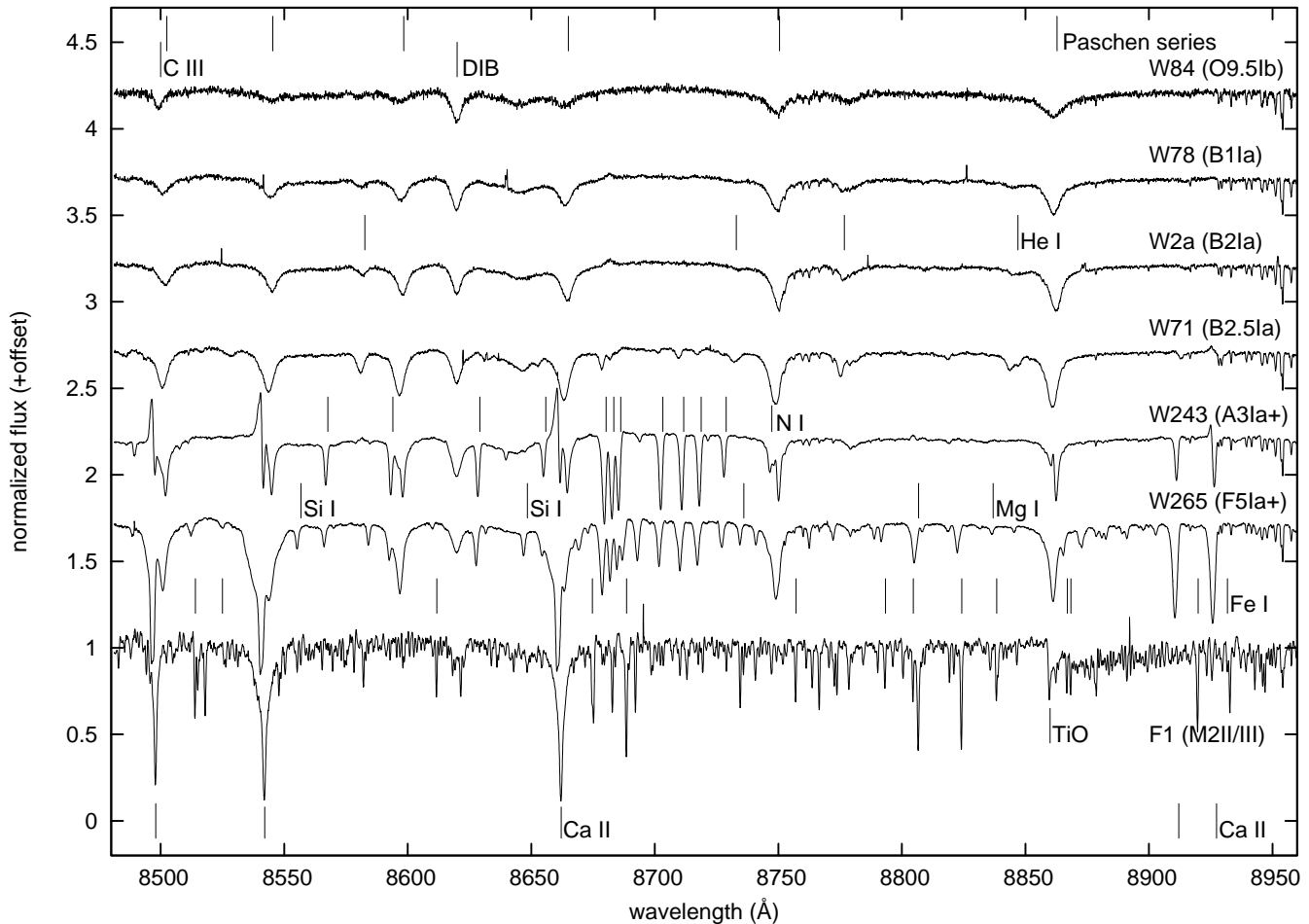


**Fig. 2.** Spectral sequence of selected targets, from the M2II/III field star F1 to the O9.5Ib cluster member W84 with the rest wavelengths of the principal absorption lines marked. Residual sky lines, as discussed in Section 2, are visible in some spectra.

using the IRAF<sup>6</sup> task *onedspec*. The signal-to-noise ratio of our co-added spectra varies with the *I*-band luminosity of the target, ranging from  $S/N > 200$  for the very luminous transitional hypergiants W243 and W265 to  $\sim 65$ – $75$  amongst the least luminous O9.5Ib targets in our *bright* sample. A master sky spectrum was created from individual fibre sky spectra, and this was subtracted from stellar spectra using the *skysub* task. Notable fibre-to-fibre variations in the sky spectra are apparent across the FLAMES field, and as a result the removal of sky lines from stellar spectra is frequently imperfect (see also discussion in Evans et al. 2005). As can be seen from Figure 2, residual sky lines are not generally significant, but in a few cases unsubtracted sky lines overlapped absorption lines used for RV measurement and had to be removed by manually interpolating between levels on either side of the emission line. Finally, spectra were corrected for heliocentric velocity using *dopcor* and normalized using the *continuum* task. A serendipitous check for zero-point errors in our data is provided by a strong, well-defined diffuse interstellar band

at  $\sim 8620\text{\AA}$  (Munari 2000). As this feature is unassociated with Wd1 it displays a constant profile and a RV that varies by less than  $\sim 1\text{km s}^{-1}$  in all spectra, implying that there are no systematic shifts in line centre or profile between epochs.

In this work only the *bright* target list is examined; a list of targets is given in Table 2 and a finder chart is plotted in Figure 1<sup>7</sup>. A representative spectral sequence, extending from the earliest objects in our *bright* sample (O9.5Ib, e.g. W84 and W234) is plotted in Figure 2 with the Paschen-series and He I lines labeled, along with the DIB at  $\sim 8620\text{\AA}$ , the C III  $\lambda 8500$  line that blends with the Pa-16 line in stars of B0.5I and earlier, and the neutral and singly-ionized metal lines that become prominent in the cooler stars. Radial velocities were determined from the strong Paschen-series and (when available) He I absorption lines, with the Pa-16  $\lambda 8502$  line excluded in stars earlier than B1I due to blending with C III  $\lambda 8500$  (this effect can be clearly seen in the bluewards shift in the Pa-16/C III blend in the O9.5Ib spectrum plotted in Figure 2). In the case of the cool hypergiants W243 and W265, the Paschen-

<sup>6</sup> IRAF is distributed by the National Optical Astronomy Observatories, which are operated by the Association of Universities for Research in Astronomy, Inc., under cooperative agreement with the National Science Foundation.

<sup>7</sup> W373 lies outside the field of view of Figure 1 and is located to the south of Wd1 16 arcseconds east of the bright field star HD151018.

series lines are frequently blended with adjacent Ca II and N I lines, and instead nine strong, unblended N I absorption lines from high-excitation multiplets ( $\chi_{\text{low}} \sim 10.2\text{eV}$ ) were used. Measurements were made in a similar manner to Bosch et al. (2009), by using the IRAF *ngausfit* task within the *stdas* package to fit Gaussian profiles to the absorption lines, with the measured stellar radial velocity at each epoch an error-weighted average of the individual absorption lines. Rest wavelengths for RV measurement are taken from the NIST Atomic Spectra database<sup>8</sup>. Errors are  $\lesssim 4\text{kms}^{-1}$  unless noted.

### 3. Results

The *bright* target list contains 16 stars that are known members of Wd1 with previously published spectral classifications (Clark et al. 2005, 2008; Negueruela et al. 2008). The previously-unclassified target W373, located to the south of Wd1 16 arcseconds from the field star HD151018, is classified as B0Iab based on the strength the Paschen-series and He I absorption lines, with a spectrum very similar to W60 (also B0Iab; Negueruela et al. 2009). Four of the five candidate targets are confirmed as members of Wd1. W3002 and W3004 display very similar spectra to W373, and are again classified as B0Iab. W3005 is slightly earlier, displaying a similar spectrum to W84 and W234 (O9.5Ib; Negueruela et al. 2009), while W3003 displays slightly broader Paschen-series lines than the B0Iab stars and is classified as B0Ib. Finally, although the fifth candidate target (F1) has a similar colour to the highly-reddened OB supergiants in Wd1, the lack of a well-defined DIB at  $8620\text{\AA}$  and the strength of the TiO  $\lambda 8860$  bandhead (Ramsey 1981) show it to be a foreground early-M giant and not a cluster member.

Table A.1 lists the measured radial velocities for the target stars. In the case of W30a, the I-band spectrum shows only very broad, weak Paschen-series absorption lines that preclude accurate measurement; we return to this in Section 4. Selected targets are examined further in the following sections. Although the detection of binaries in Wd1 is the long-term goal of our project, at this stage we are also interested in characterising possible photospheric sources of variations in RV. Both sources of variability are therefore discussed.

#### 3.1. The eclipsing binary W13

Bonanos (2007) report W13 to be a contact eclipsing binary with a 9.2-day orbital period, and it is also listed as an X-ray source with  $L_x \sim 10^{32}\text{ergs}^{-1}$  by Clark et al. (2008). Negueruela et al. (2009) classify W13 as a B0.5Ia<sup>+</sup>+OB binary, with one component being an emission-line object displaying strong H $\alpha$  emission alongside C II  $\lambda\lambda 6578, 6583$  and He I  $\lambda\lambda 6678, 7065$  lines in VLT/FLAMES LR6-mode spectra (Clark et al. 2009b). By chance, three of our observations are separated by almost integer multiples of this orbital period: the second spectrum was obtained 2.05 orbital periods after the first, while the fourth spectrum was taken after 4.98 orbital periods had elapsed. The other two are out of phase, taken after 2.71 and 7.26 orbital periods. We would therefore expect to see absorption lines at almost the same RV in three spectra with two discrepant, and this

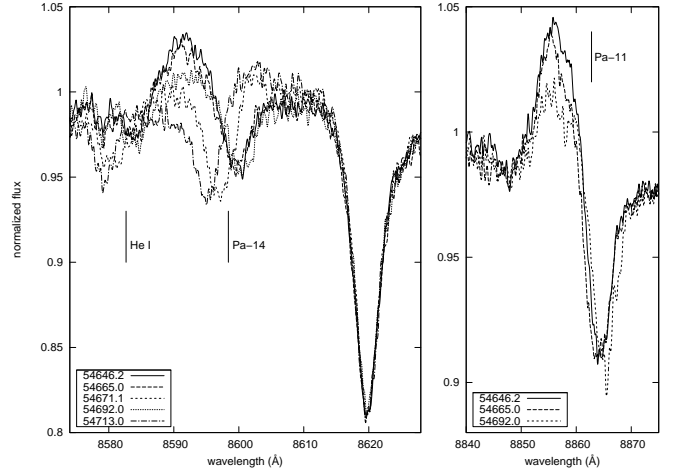


**Fig. 3.** Pa-14  $\lambda 8598$  (all five epochs, left panel) and Pa-11  $\lambda 8862$  (three epochs at near-identical phase, right panel) in the spectrum of W13. The absorption feature at  $\sim 8620\text{\AA}$  is a DIB, and rest wavelengths are marked. In this and subsequent figures the key gives the modified Julian date on which each spectrum was obtained.

can be seen in Figure 3. An emission component is seen in all Paschen-series lines, weakening noticeably between the first and fourth spectra. Weak He I absorption features are also seen, with He I  $\lambda\lambda 8583, 8777$  (van Helden 1972) most prominent. The radial velocities of the He I absorption lines closely match the absorption components of the Paschen-series lines, and although no obvious He I emission is detected in our I-band spectra the expected strength is low. Radial velocity measurements and the virtual absence of an emission line component at phase  $\sim 0.7$  (corresponding to the 24/07/2008, MJD=54671.1 spectrum) when the emission-line component is near (or at) eclipse show W13 to be a spectroscopic binary, with the emission component originating in a B0.5I<sup>+</sup>/WNVL primary and the absorption component in the secondary. The weakness of the Paschen-series absorption lines suggests a  $\sim \text{O8-9I}$  classification for the secondary, but this is inconsistent with the observed He I absorption lines which imply a later spectral type, and it is likely that there is significant infilling of the Paschen-series lines from the wind of the emission-line primary. W13 therefore appears to be an immediate precursor to the binary-rich Wolf-Rayet population in Wd1 (Crowther et al. 2006). Radial velocity measurements and orbital parameters for W13 will appear in a forthcoming paper.

#### 3.2. The Wolf-Rayet W239 (F/WR77n)

The WC9d star W239 (F/WR77n in the nomenclatures of Clark & Negueruela 2002 and van der Hucht 2006 respectively) has previously been highlighted as a likely binary due to its strong near-IR excess and hard X-ray emission (Crowther et al. 2006; Clark et al. 2008), while Dougherty & Clark (2008) report radio emission that is also consistent with a CWB. Our spectra are dominated by two strong C III  $\lambda\lambda 8500, 8664$  emission lines, with weak C IV  $\lambda 8856$  emission also apparent; the C III  $\lambda 8664$  line and nearby DIB at  $\sim 8620\text{\AA}$  are plotted in Figure 4. Significant

<sup>8</sup> [http://physics.nist.gov/PhysRefData/ASD/lines\\_form.html](http://physics.nist.gov/PhysRefData/ASD/lines_form.html)

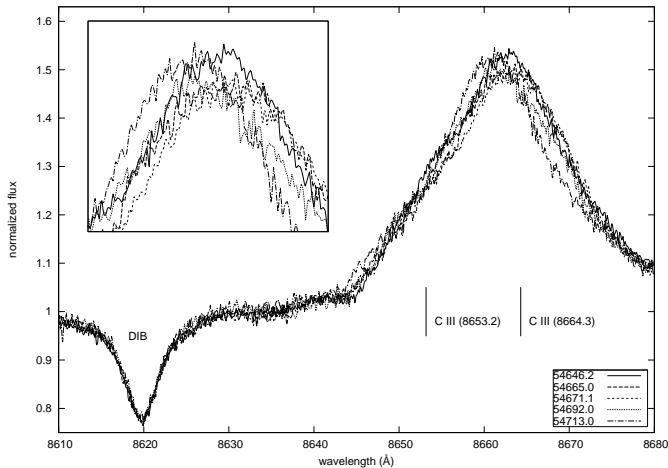


**Fig. 4.** C III  $\lambda 8664$  and the adjacent  $\sim 8620\text{\AA}$  DIB in the Wolf-Rayet W239/F. A secondary component at  $\lambda 8653$  responsible for the extended wing bluewards of the main emission peak is also marked.

radial velocity changes are apparent in all three emission lines, although the measured values of the two C III lines generally differ by  $\sim 20\text{--}40\text{km s}^{-1}$ , a result of excess emission on the redwards side of the C III  $\lambda 8500$  line shifting the profile fit relative to C III  $\lambda 8664$  and also possibly the influence of a weak secondary component at  $8653\text{\AA}$  shifting the C III  $\lambda 8664$  fit bluewards. Measurement is also complicated by the emission line profiles, which are sometimes skewed or weakly double-peaked. However, over the course of our observations RVs measured from the C III  $\lambda 8664$  line span a range of  $-82\text{km s}^{-1}$  to  $+14\text{km s}^{-1}$ , with the C III  $\lambda 8500$  line giving a very similar overall range that is redshifted by  $\sim 25\text{km s}^{-1}$  (errors estimated at  $\lesssim 10\text{km s}^{-1}$  in both cases), with a large delta of  $\sim 65\text{km s}^{-1}$  between the 24/07/2008 (MJD=54671.1) and 14/08/2008 (MJD=54692.0) spectra. Although WRs typically display low-level variability in emission lines due to clumping in the wind, the RV changes seen here are strongly suggestive of binarity. Dust-forming WC stars are generally considered to be binary systems with an OB companion (e.g. Tuthill et al. 1999), and the observed RVs are consistent with a  $\sim 15M_{\odot}$  WR primary (Crowther et al. 2006) and more massive OB secondary in a short-period orbit viewed at moderate inclination (unlike B/WR77o, eclipses are not visible in W239; Bonanos 2007). The limited sampling of our five epochs precludes estimation of an orbital period, but our long-term dataset will allow us to constrain the orbital parameters of W239.

### 3.3. The spectroscopic (candidate) binaries W2a, W43a, W234 and W3003

Figure 5 plots the Pa-14  $\lambda 8598$  line and the adjacent DIB at  $8620\text{\AA}$  for W2a and W43a, with both objects displaying notable RV variations in the photospheric absorption lines. W43a is unambiguously a short-period binary, with the measured radial velocities spanning a range of  $\sim 140\text{km s}^{-1}$  and including a delta of  $\sim 131\text{km s}^{-1}$  in the space of six days between 18/07/2008 (MJD=54665.0) and 24/07/2008 (MJD=54671.1). No eclipses are reported by Bonanos (2007), but the relatively high radial velocities suggest that

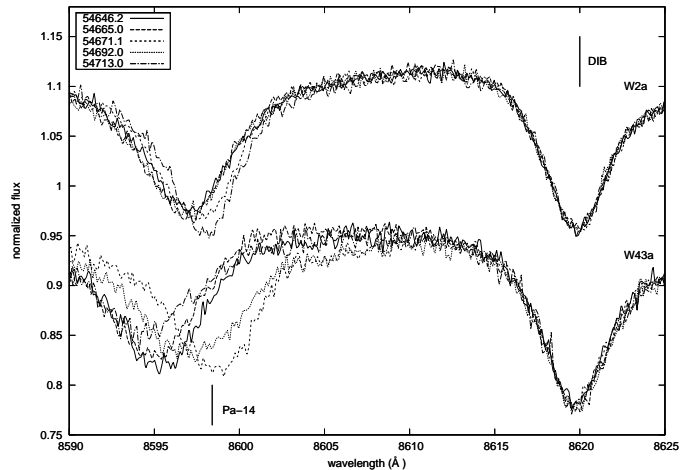


**Fig. 5.** Pa-14  $\lambda 8598$  and adjacent  $\sim 8620\text{\AA}$  DIB in the spectrum of W2a (top) and W43a (bottom). The Pa-14 rest wavelength marked. W234 and W3003, the two other candidate binaries discussed in the text, are omitted for clarity and are intermediate between the two plotted spectra.

the system must be near the  $\sin i \sim 0.7$  limit where eclipses would become visible. The  $\sim 35M_{\odot}$  initial mass of the B0Ia primary requires a massive companion to produce the observed RV changes, and although there is not direct spectroscopic evidence for this secondary, changes in the He I line profiles are tentatively suggestive of an OB companion. However, we note that changes in the Paschen-series absorption line strengths are also apparent in our spectra, and it seems likely that we are also observing photospheric variations superimposed on the changes in line centre due to orbital motion. This may explain changes in the He I profile, and follow-up observations at other wavelengths may be required to identify the companion. Nevertheless, W43a represents an encouraging prospect for accurate parameter estimation as further data become available.

W234 is duplicated on the *bright* and *faint1* lists and therefore observed on seven occasions. The overall range of observed RVs is far smaller than W43a ( $\sim 36\text{km s}^{-1}$ ), but relatively rapid RV changes are again present with spectra from 18/07/2008 (MJD=54665.0) and 24/07/2008 (MJD=54671.1) showing a delta of  $\sim 35\text{km s}^{-1}$ . This is large for bulk photospheric motions in the Paschen-series line forming region, and it is more likely that W234 is a similar short-period binary to W43a but viewed at a less favourable angle for RV measurement. W2a displays RVs ranging from  $-56.2\text{km s}^{-1}$  to  $-18.6\text{km s}^{-1}$  over the course of our observations, including a change of  $\sim 22\text{km s}^{-1}$  within the six days separating the 18/07/2008 (MJD=54665.0) and 24/07/2008 (MJD=54671.1) spectra, and a change of  $\sim 36\text{km s}^{-1}$  between the final two spectra. The variability on short timescales is less pronounced than in W234, but the amplitude of the RV changes is still large relative to the majority of our sample. However, we cannot categorically rule out a photospheric origin for these variations and classify W234 as a *probable* binary based on the magnitude of its short-term RV changes and W2a as a *candidate* binary pending further observation.

Finally, the newly-confirmed cluster member W3003 displays RVs spanning  $\sim 50\text{km s}^{-1}$  over the course of our

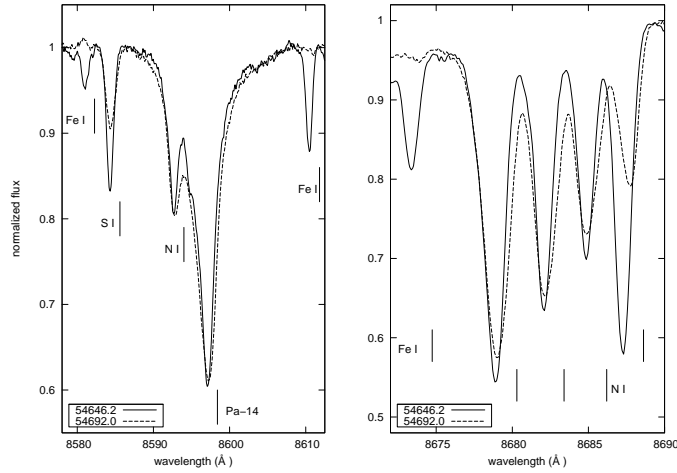


**Fig. 6.** Spectral variability in W265. The left panel plots the region around the Pa-14  $\lambda 8598$  line, while the right panel plots the region around the N I triplet at  $\lambda 8680\dots 6$ . Rest wavelengths are indicated.

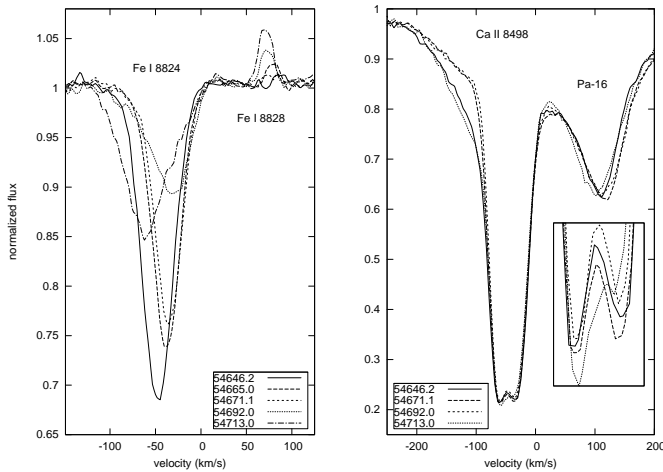


**Fig. 7.** Spectral variability in W265. The left panel plots Fe I  $\lambda 8824$  (multiplet 60) and  $\lambda 8828$  (multiplet 1269), with velocities relative to the Fe I  $\lambda 8824$  rest wavelength. The right panel plots the Ca II  $\lambda 8498$ /Pa-16  $\lambda 8503$  blend, with velocities relative to the Ca II  $\lambda 8498$  rest wavelength.

observations. Unlike the other short-period (candidate) binaries identified here, W3003 shows no rapid deltas in RV but increases from  $-4.4\text{kms}^{-1}$  in the first spectrum (29/06/2008, MJD=54646.2) to  $-54.6\text{kms}^{-1}$  in the third (24/07/2008, MJD=54671.1) before turning around and decreasing to  $-10.6\text{kms}^{-1}$  in the final spectrum (04/09/2008, MJD=54713.0). Like W234, additional observations are required to confirm the binary nature of the system, but the pattern of RV changes appears best explained by a limited sampling of a longer-period orbit viewed at moderate inclination. We therefore classify W3003 as a second *probable* binary.

### 3.4. The pulsating hypergiants W243 and W265

W243 (LBV  $\sim A3\text{Ia}^+$ ; Ritchie et al. 2009) and W265 (F5Ia $^+$ ; Clark et al. 2005) represent two of the population of cool hypergiants in Wd1. Turning first to the yellow hypergiant W265, the VLT/FLAMES spectra reveal pronounced spectral variability in the neutral metal lines, and in particular in low-excitation multiplets of Fe I, Mg I and Si I. This can be seen in Figure 6, which plots the regions around the Pa-14  $\lambda 8598$  line and the N I triplet at  $\sim 8683\text{\AA}$  on two epochs, separated by  $\sim 46$  days, that correspond approximately to apparent minimum and maximum  $T_{\text{eff}}$  (29/06/2008, MJD=54646.2 and 14/08/2008, MJD=54692.0 respectively). The first spectrum displays strong Fe I lines from multiplets 60 ( $a^5P-z^5P^o$ ,  $\chi_{\text{low}} \sim 2.2\text{eV}$ ), 339 ( $b^3P-z^3P^o$ ,  $\chi_{\text{low}} \sim 2.8\text{eV}$ ) and 401 ( $b^3G-z^3G^o$ ,  $\chi_{\text{low}} \sim 3\text{eV}$ ), but in the later spectrum the multiplet 60 line ( $\lambda 8689$ ) has weakened substantially while the multiplet 339 lines ( $\lambda\lambda 8611, 8675$ ) are undetectable and the multiplet 401 line ( $\lambda 8582$ ) is weakly in emission. This pattern continues in the left panel of Figure 7<sup>9</sup>, which plots the adjacent Fe I  $\lambda 8824$  (multiplet 60) and  $\lambda 8828$  (multiplet 1269,  $x^5D^o-e^3D$ ,  $\chi_{\text{low}} \sim 4.9\text{eV}$ ) lines over all five VLT/FLAMES epochs. Once again, the multiplet 60 line is seen to vary significantly in both strength and profile, while the multiplet 1269 line strengthens in emission. In contrast, the N I, Ca II and Pa-16 lines visible in Figures 6 and 7 display much less variability. The Fe I lines ( $\chi_{\text{low}} \sim 2-3\text{eV}$ ) and Mg I lines ( $\chi_{\text{low}} \sim 4\text{eV}$ ) form in the upper photosphere, while the N I ( $\chi_{\text{low}} \sim 10\text{eV}$ ) and Paschen-series form at lower levels. Notable differences between the two layers are apparent in Figure 8, which plots the measured radial velocities of two low-excitation and two high-excitation lines over the course of our observations. The outer photosphere, traced by low-excitation Fe I and Mg I lines, displays a pronounced infall followed by rapid expansion in the final epoch. The observed minima in the strengths of the Fe I absorption lines corresponds to maximum infall (and presumably maximum  $T_{\text{eff}}$ ), with these lines subsequently broadening due to the rapid expansion in the final epoch. In contrast the lower layers of the photosphere are more stable, and although all species display similar radial velocities during the initial infall phase, the high-excitation lines show contraction ending earlier with a less pronounced expansion in the final epoch.

The behaviour of the Fe I lines is remarkably similar to the well-studied YHG  $\rho$  Cassiopeia (Lobel et al. 2003), with the multiplet 60 line in Figure 7 developing a similar triangular profile with excess absorption in the blue wing<sup>10</sup> to that reported by Lobel et al. (1998) for the low-excitation Fe I  $\lambda 5572.8$  line. Our limited spectral coverage prevents us from examining other low-excitation absorption lines used by Lobel et al. (1998) to interpret the spectrum of  $\rho$  Cas, but, given the similarities, it is likely the Fe I lines share a common origin in a (non-radially) pulsating photosphere.

<sup>9</sup> Note that for clarity only four epochs of data are shown in the right panel, with the omitted 17/08/2008 (MJD=54665.0) profile very similar to the plotted profile from 24/08/2008 (MJD=54671.1).

<sup>10</sup> The excess blue-wing absorption forms in a cool, optically-thick expanding wind at smaller optical depth (Lobel et al. 2003).



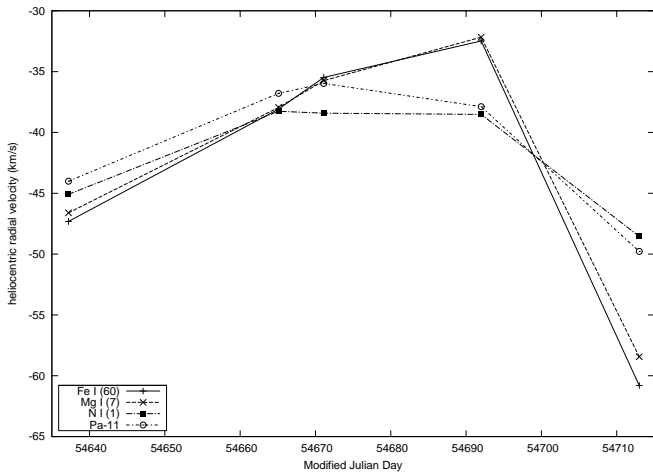


**Fig. 8.** Heliocentric radial velocity changes in low- and high-excitation absorption lines in W265. Plotted are Fe I (multiplet 60,  $\chi_{\text{low}} \sim 2.2\text{eV}$ ), Mg I (multiplet 7,  $\chi_{\text{low}} \sim 4.3\text{eV}$ ), N I (multiplet 1,  $\chi_{\text{low}} \sim 10.2\text{eV}$ ) and the Paschen-11 line ( $\chi_{\text{low}} = 12.04\text{eV}$ ). Errors are  $\sim \pm 2\text{kms}^{-1}$ .

Finally, we note the weak emission evident in the core of the strong Ca II  $\lambda 8498$  line in Figure 7; a similar effect is seen in the core of the other Ca II  $\lambda\lambda 8542, 8662$  multiplet-2 lines, but in these cases infilling of the line centre redwards of the emission peak is seen, leading to an asymmetric core profile. The  $4^2\text{P}^{\circ}$  ( $\chi_{\text{low}} \sim 1.7\text{eV}$ ) lower level of the near-IR Ca II triplet is fed by the Ca II-K and -H lines in the near-UV, and core emission in the Fraunhofer lines is an indicator of chromospheric activity in cool stars. Such cores are reported in  $\alpha$  Orionis but are not observed in the near-IR triplet (Lobel & Dupree 2000), implying a higher chromospheric temperature in W265. Observations of  $\rho$  Cas show that core emission in the chromospheric Ca II-H and K lines is not constant (Lobel et al. 2003), implying that a permanent chromosphere is not present, and this may also be the case for W265; no apparent chromospheric X-ray emission was detected (Clark et al. 2008, section 4.2.3), suggesting that the chromospheric activity implied by the Ca II lines may also be transitory. Further observation and modeling of W265 is required to determine the origin of these features. Lobel et al. (2003) report line-splitting in low-excitation ( $\chi_{\text{low}} \leq 1.5\text{eV}$ ) Fe I multiplets and other low-excitation metals. However, our limited spectral coverage precludes examination of the multiplets in which splitting is reported. Sargent (1961) lists Fe I multiplet 60 as containing double lines in  $\rho$  Cas, but no evidence of core doubling in this multiplet is seen in our spectra of W265.

Significant pulsational variability is also observed in W243. The highly-variable Fe I lines observed in W265 are not present in the hotter LBV ( $\text{A3Ia}^+$ ), which displays a complex Fe II spectrum along with absorption lines from other neutral and singly-ionized metals and an emission-line spectrum containing Balmer- and Paschen-series lines, He I and Ca II. This emission-line spectrum is a result of a hot companion star ionizing the wind of the LBV primary (Ritchie et al. 2009), but this is not directly reflected in the cool-state absorption lines which display radial velocities in a narrow range of  $-45\text{kms}^{-1}$  to  $-15\text{kms}^{-1}$  across ten epochs of VLT/UVES and VLT/FLAMES data. These lines

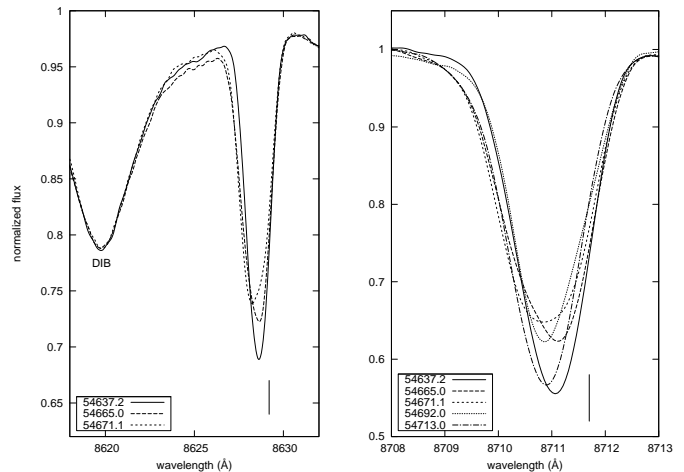


**Fig. 9.** Spectral variability in the LBV W243. The left panel plots N I  $\lambda 8629$  line and adjacent  $\sim 8620\text{\AA}$  DIB from three epochs (with the other two omitted for clarity) while the right panel plots the N I  $\lambda 8712$  line from all five epochs. Rest wavelengths are marked.

display RV variations on timescales of days, but - if they were due to orbital motion - we would expect a much wider range of radial velocities than observed unless, by chance, we are observing the system from almost directly above the orbital plane. The variations are most clearly seen in the Si II  $\lambda\lambda 6349, 6371$  doublet (obtained using VLT/UVES with cross-disperser #3,  $R \sim 40,000$ ) and in the near-IR N I lines; an example of the latter is shown in Figure 9. In addition, VLT/UVES observations of the N I lines reveal the formation of excess bluewards absorption similar to that seen in the Fe I multiplet 60 line in W265 at a time when Fe II emission lines develop pronounced P-cygni profiles indicating enhanced mass loss. W243 therefore appears to be undergoing very similar pulsational mass-loss to W265, albeit at higher  $T_{\text{eff}}$ ; we examine the spectrum of W243 in detail in Ritchie et al. (2009).

### 3.5. The early-B supergiants

Statistically-significant RV changes are also apparent in a number of the early-B supergiants, including W8b, W21, W23a, W71 and W3004. Of these, W71 (B2.5Ia; Negueruela et al. 2009) is one of the latest of the continuous sequence of OB supergiants in Wd1, displaying strong Paschen-series and He I absorption lines along with weak N I lines indicative of its cooler state. W8b and W23a are slightly earlier, displaying no apparent N I lines. Finally, W21 and W3004 are the earliest of this group, with spectral types B0.5Ia and B0Iab respectively. With the exception of W8b all are listed as aperiodic variables by Bonanos (2007), and none are significant detections at X-ray wavelengths (Clark et al. 2008).

In all cases, the observed RV variations lie in a narrow range of  $\sim 15\text{--}25\text{kms}^{-1}$  with no rapid variations between epochs. Although this is compatible with longer-period orbital motion, the radial velocity changes in the Paschen-series lines are accompanied by changes in absorption line strength and profile, and it is more likely that the origin of the RV changes is photospheric. This is best illustrated by

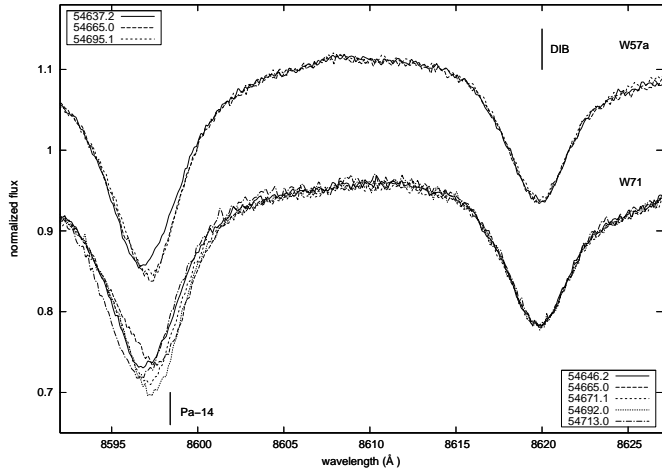


**Fig. 10.** The Pa-14  $\lambda 8598$  line and adjacent  $\sim 8620\text{\AA}$  DIB in the spectrum of W57a (top) and W71 (bottom). The rest wavelength of Pa-14 is marked.

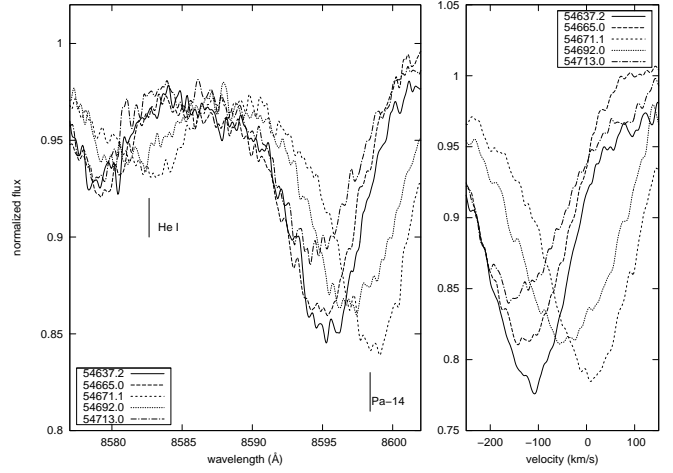


**Fig. 12.** As Figure 11, but showing variations in the Paschen-series absorption lines in the short-period binary W43a.

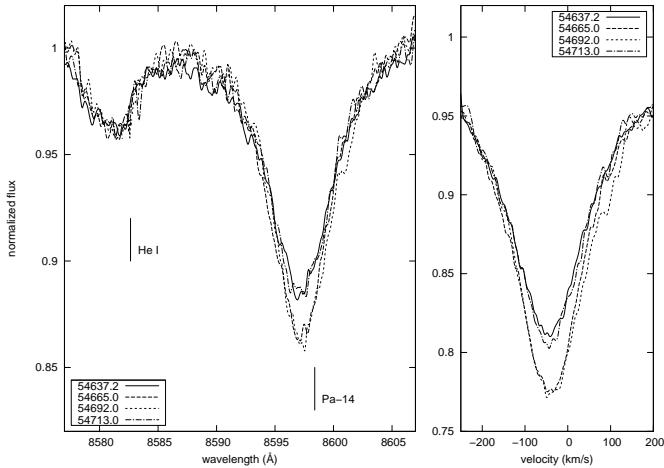


**Fig. 11.** Variations in the Paschen-series absorption lines in W78. The left panel plots the Pa-14  $\lambda 8598$  line and adjacent He I  $\lambda 8583$  line, with rest wavelengths marked, while the right panel plots the Pa-11  $\lambda 8862$  line with velocities relative to its rest wavelength.

W71 and the cooler transitional supergiant W57a (B4Ia; Negueruela et al. 2009) which is included in the *faint1* list and was observed on three occasions; both are plotted in Figure 10. As well as variations in the Paschen-series lines, both objects also show pronounced changes in the strength of the N I  $\lambda 8680$  triplet over the course of our observations, a sensitive indicator of temperature that strengthens rapidly from B2Ia to B4Ia (Negueruela et al. 2009) and is therefore strongly suggestive of photospheric changes. In addition, W78 (B1Ia) does not display statistically significant RV changes ( $\lesssim 10\text{ km s}^{-1}$  during the course of our observations) but nevertheless displays notable changes in the strength of the Paschen-series absorption lines. These changes, plotted in Figure 11, are not apparent in the adjacent He I line which again suggests a photospheric origin. Radial velocity or line profile changes are therefore observed in *all* stars later than  $\sim B0.5\text{Ia}$  in our sample, and it is possi-

ble that the early- to mid-B supergiants in our sample all lie within a region of pulsational instability that extends to the cool hypergiants (Maeder & Rufener 1972; Schaller 1990). Unless the stars are short-period binaries at favourable inclination (as with W43a, which displays clear signs of *both* orbital and pulsational variations; see Figure 12) we cannot conclusively detect binarity with our short baseline of observations, although the longer baseline survey will be sensitive to long-term trends in these objects.

## 4. Discussion and Conclusions

### 4.1. Binary detections

In this work we present first-epoch results from a VLT/FLAMES radial velocity survey designed to identify high-mass binaries in the starburst cluster Westerlund 1. As expected, large RV changes are detected in the short-period eclipsing binary W13 (Bonanos 2007) which displays variable emission from a B0.5Ia<sup>+</sup>/WNLV emission line primary and He I and infilled Paschen-series absorption in an early-B secondary. As such, it appears to represent the immediate evolutionary precursor to the binary-rich Wolf-Rayet population in Wd1, such as the eclipsing binary B/WR77o (Bonanos 2007). The WC9d star W239 (F/WR77n) also shows significant RV changes compatible with a short-period WR+OB CWB viewed at moderate inclination: the OB secondary is already strongly implied by the presence of hot dust (Crowther et al. 2006), hard X-ray emission (also seen in W13; Clark et al. 2008) and non-thermal radio emission (Dougherty & Clark 2008). In addition we identify W43a as a new short-period binary with a massive, so-far unresolved companion. W234 and W3003 are probable binaries, and W2a is a strong candidate binary. Both W2a and W234 appear to be short-period binaries, with W234, at spectral type O9.5Ib, earlier than the apparently pulsationally-variable early-B supergiants discussed in Section 3.5. Finally, the measured RVs for W3003 are consistent with limited sampling of a short- or longer-period binary. Future observations will resolve the nature of these systems.

An second important group of objects in the context of our RV survey are W6a, W15, W17 (included in the *faint* lists) and W30a, which have all been identified as strong binary candidates in previous studies of Wd1. W30a is the strongest X-ray source in Wd1 after the magnetar CXOU J164710.2-455216 (Clark et al. 2008) and a factor of  $\sim 10$  more luminous than would be expected from a single star<sup>11</sup>, while W6a is a periodic variable (Bonanos 2007) that is also a hard X-ray source. Both display almost featureless I-band spectra with very broad, shallow Paschen-series absorption lines typical of spectroscopic binaries (see also Negueruela et al. 2009) and broad, variable H $\alpha$  emission (Clark et al. 2008). W15 and W17 are both detected at radio (Dougherty & Clark 2008) wavelengths: the spectral index of W15 suggests composite stellar+non-thermal emission<sup>12</sup>, while the index of W17 is unambiguously non-thermal. The radio observations therefore suggest that both are CWBs, although they are only weak detections at X-ray wavelengths (Clark et al. 2008). None of these objects show significant RV variations in our data. In the case of W6 and W30a this is unsurprising, as the broad, weak I-band spectral features are insensitive to changes in RV due to the difficulty in determining the line centre, although at favourable inclination the large RV changes expected of a short-period, high-mass binary would still be apparent. In contrast, W15 and W17 display well-defined Paschen-series absorption lines but no significant variations in RV. However, in these cases it is likely that wider orbits are required in order for non-thermal radio emission to be detectable, and the relatively short baseline of our first observations remains insensitive to longer-period, radio-strong binaries.

Radial velocity surveys are also expected to be incomplete, as a subset of objects will be viewed at unsuitable orbital inclinations while others do not display spectra that allow accurate RV measurement. There is also an element of chance in conclusively detecting binarity from a limited number of RV measurements, as is apparent from the observations of W13 and W43a: only one of five observations W43a unambiguously identifies it as binary, while by chance three observations of W13 fall at almost exactly the same orbital phase. However, while the short-period binary W13 was detected photometrically (Bonanos 2007) and was also as a strong binary candidate from spectroscopic (Negueruela et al. 2009) and X-ray (Clark et al. 2008) surveys, neither W43a or the probable/candidate binaries W2a, W234 and W3003 have been identified in previous work. Therefore, although the principle aim of our VLT/FLAMES survey is to build a dataset that is sensitive to long-period binaries, there is also great value to close-spaced RV measurements (e.g. the pair from 18/07/2008, MJD=54665.0 and 24/07/2008, MJD=54671.1, separated by six days) that effectively detect short-period binaries that are not apparent from photometry or single-epoch spectroscopy.

<sup>11</sup> The optical spectrum of W30a is also indicative of an interacting binary (Clark et al. 2008).

<sup>12</sup> Purely thermal emission from W15 would imply a very high mass loss rate inconsistent with the observed spectral type.

#### 4.2. Pulsations and the cluster velocity dispersion

The cool hypergiants W243 and W265 are both undergoing photospheric pulsations, with W265 showing strong spectroscopic similarities with the non-radially pulsating yellow hypergiant  $\rho$  Cas (Lobel et al. 2003). Chromospheric activity is also apparent from core emission in the near-IR Ca II triplet. We also find significant RV variations of  $\sim 15$ – $25$  km s<sup>-1</sup> in five early-B targets: while these could be orbital, in *all* targets later than spectral type  $\sim$ B1Ia these RV changes are accompanied by changes in absorption line profile suggestive of photospheric pulsations. The two-month baseline of our initial data offers prevents us from distinguishing a limited sampling of a long-period orbit from photospheric pulsations in the early-B supergiants, and further observations are required to break this degeneracy. However, regardless of their origin, these variations imply that care must be taken in deriving a stellar velocity dispersion for Wd1 from a single epoch of data. Bosch et al. (2009) find that the binary population leads to a significant overestimation of the velocity dispersion for NGC 2070 unless binaries are removed from the sample, and the pulsational variations reported here may have a similar effect on infra-red determinations of the velocity dispersion for Wd1 (e.g. Mengel & Tacconi-Garman 2008). We note that separate VLT/FLAMES observations of the F2Ia<sup>+</sup> YHG W4 also reveal apparent pulsational variations in the Fe I lines (Clark et al. 2009b) and consider it likely that photospheric pulsations are a general characteristic of the transitional B-type supergiant and cool hypergiant populations of Wd1.

#### 4.3. Binary fraction

Despite the expected limitations of our short-baseline initial dataset, the results presented here support the high binary fraction implied from the earlier photometric and multiwavelength observations of Wd1. Considering just the sample presented here, RV measurements show W13, W239 and W43a are binaries with W234, W3003 and W2a likely candidates. Radio and X-ray measurements strongly suggest a further four targets (W6, W15, W17 and W30a) *are* binaries but RV variations are undetected - and, in two cases, potentially undetectable - in our VLT/FLAMES data. Any signature of orbital motion in the two cool hypergiants is masked by photospheric pulsations, but the LBV W243 requires a hot companion to produce the observed He I and Ly $\alpha$ -pumped Fe II and O I emission lines that are incompatible with the cool-phase LBV primary (Ritchie et al. 2009). The YHG W265 is also plausibly binary, being associated with a compact, resolved radio source (Dougherty & Clark 2008) which could not be ionized by the YHG itself. While the source of ionizing photons could simply be the OB supergiant population of Wd1, the YHG HR 8752 is also detected at radio wavelengths as a result of the wind being ionized by a B1V companion (Stickland & Harmer 1978; Pitters et al. 1988). The hot companion also explains the observed [N II] emission in the spectrum of HR 8752; notably [N II]  $\lambda\lambda 6548, 6583$  emission is visible in VLT/FLAMES LR6-mode spectra of W265 (but not in the other YHGs; Clark et al. 2009b) and [N II]  $\lambda 6583$  emission was also reported by Westerlund (1987).

Therefore even a conservative estimate that includes just the robust RV detections<sup>13</sup> and the two objects that lack RV detections but have binarity strongly implied by other observations<sup>14</sup> suggests a binary fraction of 30% (6/20) amongst our initial *bright* sample of supergiant stars in Wd1, increasing to  $\geq 40\%$  if other candidate binaries are included<sup>15</sup>. Both percentages are likely to increase as more data become available. If the more evolved WR/WNVL binaries and transitional hypergiants are excluded, then we find  $\sim 19\%$  (3/16) of the OB supergiants in our sample are strong binary detections, rising to  $\sim 30\%$  (5/16) if candidates are included. Robust estimates of the binary fraction amongst the OB supergiant population of Wd1 will become available once the full FLAMES dataset is analysed in Paper II of this series. However, these values are broadly consistent with the high binary fraction in the Wolf-Rayet population (Crowther et al. 2006); future observations and Monte-Carlo simulations planned for Paper III will reveal if the binary fraction of the two populations are equivalent.

*Acknowledgements.* JSC gratefully acknowledges the support of an RCUK fellowship. IN has been funded by grants AYA2008-06166-C03-03 and Consolider-GTC CSD-2006-00070 from the Spanish Ministerio de Ciencia e Innovación (MICINN). We thank an anonymous referee for detailed and constructive comments.

## References

- Baade, D., Meisenheimer, K., Iwert, O. et al., ESO Messenger, 95, 15  
 Bonanos, A.Z. 2007, AJ, 133, 2696  
 Bonnell, I. A., Bate, M. R., Zinnecker, H., 1998, MNRAS, 289, 93  
 Bonnell, I. A., Bate, M. R., 2005, MNRAS, 362, 915  
 Bonnell, I. A., Bate, M. R., 2006, MNRAS, 370, 488  
 Bosch, G., Terlevich, E. & Terlevich, R. 2009, AJ, 137, 3437  
 Clark, J.S. & Negueruela, I. 2002, A&A, 396, L25  
 Clark, J.S., Negueruela, I., Crowther, P.A. & Goodwin, S. 2005, A&A, 434, 949  
 Clark, J.S., Muno, M.P., Negueruela, I., et al. 2008, A&A, 477, 147  
 Clark, J.S., Crowther, P.A. & Mikles, V.J. 2009a, A&A, in press, arXiv:0909.3818v1 [astro-ph.SR]  
 Clark, J.S., Ritchie, B.W. & Negueruela, I. 2009b, A&A, in prep.  
 Clark, P. C., Bonnell, I. A., 2004, MNRAS, 347, L36  
 Clarke, C. J., Bonnell, I. A., Hillenbrand, L. A., 2000, in Mannings V., Boss, A. P., Russell, S. S., eds, Protostars and Planets IV., Univ. Arizona Press, Tucson, p. 151  
 Crowther, P.A., Hadfield, L.J., Clark, J.S., Negueruela, I. & Vacca, W.D. 2006, MNRAS, 372, 1407  
 Davies, M. B., Bate, M. R., Bonnell, I. A., Bailey, V. C., Tout, C. A., 2006, MNRAS, 370, 2038  
 Dougherty, S.M. & Clark, J.S. 2008 in: Massive Stars: Fundamental Parameters and Circumstellar Interactions, RMxAC, 33, 68  
 Evans, C.J., Smartt, S.J., Lee, J.-K. et al. 2005, A&A, 437, 467  
 García, B., Mermilliod, J. C., 2001, A&A, 368, 122  
 van der Hucht 2006, A&A, 458, 453  
 Howarth, I. D., Murray, J., Mills, D., & Berry, D. S. 2003, in Starlink User Note 50.24, Rutherford Appleton Laboratory  
 Kiminki, D. C., Kobulnicky, H. A., Kinemuchi, K., et al., 2007, ApJ, 664, 1102  
 Kobulnicky, H.A. & Fryer, C.L. 2007, ApJ, 670, 747  
 Lobel, A. & Dupree, A.K. 2000, ApJ, 545, 454  
 Lobel, A., Israelian, G., de Jager, C. et al. 1998, A&A, 330, 659  
 Lobel, A., Dupree, A.K., Stefanik, R.P. et al. 2003, ApJ, 583, 923  
 Maeder, A. & Rufener, F. 1972, A&A, 20, 437  
 Mengel, S. & Tacconi-Garman, L.E. 2008 in: proceedings of the meeting young massive star clusters - initial conditions and environments, arXiv:0803.4471  
 Moore, C.E. 1945, A multiplet table of astrophysical interest, Contribution from the Princeton University Observatory No. 20  
 Munari, U. 2000 in: Molecules in Space and in the Laboratory, Italian Phys. Soc., 67, 179  
 Negueruela, I., Clark, J.S., Hadfield, L.J. & Crowther, P.A. 2008 in: Massive Stars as Cosmic Engines, Proceedings of the International Astronomical Union, IAU Symposium, Volume 250, 301  
 Negueruela, I., Clark, J.S., et al. 2009, A&A, in prep.  
 Pasquani, L., Avila, G., Blecha, A., et al. 2002, The Messenger, 110, 1  
 Pitters, A., de Jager, C., Nieuwenhuijzen, H. 1988, A&A, 196, 115  
 Ramsey, L.W. 1981, AJ, 86, 557  
 Rauw, G., Crowther, P. A., De Becker, M., et al., 2005, A&A, 432, 985  
 Ritchie, B.W., Clark, J.S., Negueruela, I. & Najarro, F. 2009, A&A, in press, arXiv:0910.0529v1 [astro-ph.SR].  
 Sargent, W.L. 1961, ApJ, 134, 142  
 Sana, H., Antokhina, E., Royer, P., et al. 2005, A&A, 441, 213  
 Sana, H., Gosset, E., Naze, Y., Rauw, G., Linder, N., 2008, MNRAS, 386, 447  
 Schaller, G. 1990 in: confrontation between stellar pulsation and evolution, ASP Conf. Ser. 11, 300  
 Schnurr, O., Casoli, J., Chené, A.-N., Moffat, A.F.J. & St-Louis, N. 2008, 389, L38  
 Skinner, S.L., Perna, R. & Zhekov, S.A. 2006, ApJ, 653, 587  
 Stickland, D.J. & Harmer, D.L. 1978, A&A, 70, L53  
 Tuthill, P.G., Monnier, J.D. & Danchi, W.C. 1999, Nature, 398, 487  
 van Helden, R. 1972, A&A, 19, 388  
 Westerlund, B.E. 1961, PASP, 73, 51  
 Westerlund, B.E. 1987, A&AS, 70, 311  
 Yorke, H., Sonnhalter, C., 2002, ApJ, 569, 846  
 Zinnecker H., McCaughrean, M. J., Wilking, B. A., 1993, in Levy E. H., Lunine, J. I., eds, Protostars and Planets III. UNiv. Arizona Press, Tucson, p.429

## Appendix A: Radial Velocity measurements

<sup>13</sup> W13, W43a, W239 and W3003.

<sup>14</sup> W30a, a strong X-ray and spectroscopic binary candidate, (Clark et al. 2008), and W243, which displays an emission line spectrum incompatible with an isolated cool hypergiant, (Ritchie et al. 2009).

<sup>15</sup> W6a, W15 and W17 are not included in these percentages, as they are specifically selected from the *faint* lists as objects we believe to be binary but do not show RV changes in our initial data.

**Table A.1.** Error-weighted radial velocity measurements for the targets listed in Table 2.<sup>a,b</sup>

ID	Epochs	Line(s) <sup>c</sup>	Range <sup>d</sup> (kms <sup>-1</sup> )	Modified Julian Date							Notes
				54637	54646	54665	54671	54692	54695	54713	
W2a	5	Pa11-16, He I	-51.0 - -14.1	-	-49.3	-56.2	-33.9	-54.1	-	-18.6	Cand. binary
W8b	5	Pa11-16	-61.6 - -40.3	-	-61.6	-49.9	-40.3	-47.4	-	-50.7	
W21	5	Pa11-14	-57.4 - -31.1	-	-57.4	-35.0	-43.1	-55.1	-	-31.1	Binary
W23a	5	Pa11-16	-62.4 - -42.9	-	-47.9	-55.6	-56.6	-42.9	-	-62.4	
W43a	5	Pa11-14	-137.9 - +8.1	-	-109.7	-123.1	+8.1	-38.8	-	-137.9	
W55 <sup>e</sup>	7	Pa11-14	-	-43.1	-49.9	-55.4	-45.4	-43.8	-53.9	-55.5	
W60 <sup>e</sup>	5	Pa11-14	-	-	-40.5	-48.3	-45.8	-48.2	-	-37.7	
W71	7	Pa11-16, He I	-61.9 - -38.7	-57.3	-52.9	-39.4	-47.3	-44.8	-46.4	-62.4	Puls. BSG
W78	5	Pa11-15	-	-	-46.7	-46.4	-41.3	-39.9	-	-49.5	
W84	5	Pa11-13	-	-	-53.8	-59.0	-54.9	-54.6	-	-55.8	
W234 <sup>e</sup>	7	Pa11-13	-67.0 - -30.8	-67.0	-66.9	-66.2	-30.8	-46.4	-56.9	-32.7	Prob. binary
W239 <sup>f</sup>	5	C III $\lambda$ 8664	-81.6 - +14.1	-	-26.9	-10.7	+14.1	-49.7	-	-81.6	Wolf-Rayet
W243 <sup>g</sup>	5	N I (1 & 8)	-28.8 - -20.4	-	-22.7	-20.4	-27.7	-28.3	-	-28.8	Puls. LBV
W265 <sup>g</sup>	5	N I (1 & 8)	N/A <sup>h</sup>	-	-47.6	-36.8	-36.0	-37.9	-	-49.8	Puls. YHG
W373 <sup>e</sup>	5	Pa11-14	-	-	-50.8	-50.9	-45.8	-53.8	-	-52.9	Prob. binary
W3002 <sup>e</sup>	5	Pa11-14	-	-	-36.1	-38.6	-47.7	-39.4	-	-43.0	
W3003 <sup>e</sup>	5	Pa11-14	-54.6 - -4.4	-	-4.4	-43.7	-54.6	-22.0	-	-10.6	
W3004 <sup>e</sup>	5	Pa11-14	-62.3 - -35.5	-	-47.9	-62.3	-54.3	-35.5	-	-46.0	
W3005 <sup>e</sup>	5	Pa11-13	-	-	-43.9	-46.9	-52.4	-51.6	-	-49.9	

<sup>a</sup>Errors are not listed, but are  $\leq 4\text{kms}^{-1}$  for the OB supergiants,  $\leq 3\text{kms}^{-1}$  for the two cool hypergiants and  $\lesssim 10\text{kms}^{-1}$  for the Wolf-Rayet W239.

<sup>b</sup>The broad, weak Paschen-series absorption lines in W30a precluded accurate RV measurement, while RV measurements for the eclipsing binary W13 discussed in Section 3.1 will appear in a forthcoming paper.

<sup>c</sup>The line(s) used for RV measurement.

<sup>d</sup>The range of measured radial velocities is given for targets in which statistically-significant variations are detected.

<sup>e</sup> Displays a distorted Pa-16 line due to blending with C III  $\lambda$ 8500 and a weak Pa-15 line that yield discrepant radial velocities compared to the other Paschen-series lines.

<sup>f</sup> The C III  $\lambda$ 8500 and C III  $\lambda$ 8664 lines seen in the spectrum of the Wolf-Rayet W239 give discrepant RV measurements ( $\sim 25\text{kms}^{-1}$ ; see discussion in Section 3.2). The value for C III  $\lambda$ 8664 is given here.

<sup>g</sup> The cool hypergiants W243 and W265 display rich absorption-line spectra, with a large number of potential lines suitable for RV measurement. The values given here are the average of nine of the strongest unblended N I absorption lines from multiplets 1 and 8 (Moore 1945). Note that in both objects species-to-species variation in RV is seen, with clear evidence of velocity stratification in the photosphere of W265 (see discussion in text).

<sup>h</sup> The range of observed radial velocities in W265 varies depending on the absorption line used to make the measurement. See Section 3.4.